**Atmospheric
Chemistry
and Physics
Discussions**

Sea-salt particle
hygroscopic growth
and activation

D. Niedermeier et al.

Title Page

Abstract	Introduction
Conclusions	References
Tables	Figures

◀◀ ▶▶

◀ ▶

Back Close

Full Screen / Esc

Printer-friendly Version

Interactive Discussion

EGU

LACIS-measurements and parameterization of sea-salt particle hygroscopic growth and activation

D. Niedermeier, F. Stratmann, H. Wex, E. Brüggemann, A. Kiselev, H. Henk, and J. Heintzenberg

Leibniz Institute for Tropospheric Research, Permoser Str. 15, 04318 Leipzig, Germany

Correspondence to: D. Niedermeier (niederm@tropos.de)

Abstract

The Leipzig Aerosol Cloud Interaction Simulator (LACIS) was used to investigate the hygroscopic growth and activation of sea-salt particles which were generated from three different sea-water samples. Köhler theory was utilized to model the hygroscopic growth of these particles. Some parameters used in this model are unknown for sea-salt. These parameters are combined in an "ionic density" ρ_{ion}. For each sea-salt sample an average ρ_{ion} was determined by fitting the Köhler equation to the data from the hygroscopic growth measurements. LACIS was also used to measure the activation of the sea-salt particles at three different supersaturations: 0.10%, 0.16% and 0.30%. A CCN-closure was tested by calculating the critical diameters D_{crit} for the sea-salt particles at these supersaturations, using the Köhler model and the corresponding ρ_{ion} as derived from the hygroscopic growth data. These calculated critical diameters were compared to the measured ones. Measured and calculated values of D_{crit} agree within the level of uncertainty. Based on this successful closure, a new parameterization to describe sea-salt-particle hygroscopic growth (at RH>95%) and activation has been developed.

1 Introduction

Most of the earth's surface is covered by oceans. For that reason marine aerosol particles largely affect the global climate. Depending on their optical properties, marine aerosol particles scatter and absorb the incoming solar radiation and therefore influence the radiation budget of the earth (Fitzgerald, 1991). The optical properties of the particles depend on the particle size distribution, their shape and their chemical composition and through their hygroscopicity also on the ambient relative humidity (Pilinis et al., 1995; Randles et al., 2004).

Due to their hygroscopicity the marine aerosol particles act as cloud condensation nuclei (CCN). They influence the cloud droplet size distribution and hence indirectly the

radiation budget. The contribution of marine stratus and stratocumulus clouds to the earth's albedo is about 30% to 40% (Randall et al., 1984).

The marine aerosol principally consists of sea-salt, non-sea-salt (nss) sulfate particles and possibly biological particles from the ocean microlayer (Leck and Bigg, 2005a,b). Sea-salt particles are produced in a direct and an indirect way (Blanchard and Woodcock, 1957, 1980; Gong et al., 1997; O'Dowd et al., 1997). For wind speeds larger than $4\,\text{m·s}^{-1}$ waves are generated due to wind stress. These waves break and thereby sea-salt droplets with diameters greater than $10\,\mu m$ are produced (Fitzgerald, 1991). During this wave breaking process also air bubbles are introduced into the surface water. They rise and burst after reaching the surface, producing so called film and jet drops. Depending on the bubble size, about ten jet drops with an average diameter of $1–2\,\mu m$ and several hundred film drops with a diameter smaller than $1\,\mu m$ are generated (O'Dowd et al., 1997). Since the relative humidity (RH) over the ocean surface is about 98%, the generated drops evaporate until the water vapor pressure over the drop surface is equal to that of the environment (Blanchard and Woodcock, 1980).

Nss-sulfate particles also play an important role in the marine atmosphere. The main source of these particles in the remote marine boundary layer is dimethylsulfide (DMS) which is mainly produced by phytoplankton (Andreae et al., 1985; Andreae and Raemdonck, 1983). Typical nss-sulfate particle concentrations in clean marine air lie within 50 to $100\,\text{cm}^{-3}$ (O'Dowd et al., 1997). Although nss-sulfate particles are less hydrophilic than sea-salt particles, they play an important role in cloud formation processes. Measurements have shown that for small wind speeds the concentration of nss-sulfate particles in the accumulation mode, i.e., in the mode which provides most of the CCN, is larger than that of the sea-salt particles. As sea-salt particles mainly occur in the coarse-mode, it was expected that these particles contribute a negligible amount to the CCN in comparison to nss-sulfate particles (Charlson et al., 1987), because larger particles are removed from the atmosphere more quickly than smaller ones. Observations of O'Dowd and Smith (1993), however, showed that under adequate wind conditions the sea-salt particles also occur in the accumulation mode down to sizes of

EGU

100 nm. They can even dominate this size range, because the wave activity increases with increasing wind speed. More air bubbles are produced and thus more film and jet drops are generated. Over a period of low wind speeds the number concentration of sea-salt particles ranges between 5 and 30 cm^{-3} (Blanchard and Cipriano, 1987). With an increase of wind speed to 17 m·s^{-1} the concentration in the accumulation mode may exceed 70 cm^{-3} (O'Dowd et al., 1997). Due to updrafts, sea-salt particles are transported up to the cloud base and consequently even under moderate meteorological conditions more than 90% of the activated CCN in marine stratocumulus clouds may consist of sea-salt (O'Dowd et al., 1997).

As mentioned above, marine aerosol particles mainly consist of hygroscopic particles. Thereby the scattering of the incoming solar radiation depends on the ambient relative humidity, because the amount of the scattered light is related to the particle size. The particle diameters change with relative humidity, depending on the hygroscopic properties of the particles. To include the influences of sea-salt particles on scattering and cloud formation into numerical models, measurements of hygroscopic growth and activation are required. In this context it is also relevant, whether or not possible differences in the chemical composition of the oceans and therefore of the sea-salt particles influence the hygroscopic growth and activation behavior. For that reason sea-salt particles from three different sea-water samples were investigated regarding their hygroscopic growth and activation to cloud droplets. For the investigations the Leipzig Aerosol Cloud Interaction Simulator (LACIS, Stratmann et al. (2004)) was used. LACIS is a laminar flow tube that can operate at a stable RH, which can be adjusted from almost 0% up to larger than 99% (Wex et al., 2005). It can also be used at supersaturations from 0.1% up to several percent.

For this study the hygroscopic growth of the different sea-salt particles was measured in a RH range from 79.8% up to 98.8% (For the first time, measurements were performed at this high RH on sea-salt particles). It was investigated whether differences in the chemical composition cause differences in the hygroscopic behavior. Furthermore, the measured grown diameters were compared to the growth of pure sodium chloride

Sea-salt particle hygroscopic growth and activation

D. Niedermeier et al.

EGU

particles. Dry NaCl particles possess a cubical shape. Since the main component of the three different sea-salt samples is NaCl, it was investigated if a shape factor has to be taken into account for the generated sea-salt particles.

For the activation measurements of the sea-salt particles, supersaturations similar to those observed at the base of marine stratocumulus clouds (0.1% to 0.3%, Hudson and Frisbie, 1991) were used. Critical particle diameters were determined for the three different sea-salt samples and for pure NaCl.

In addition, a CCN-closure was tested for different sea-salt particles and for NaCl. For that purpose, the measured hygroscopic growth was used with Köhler theory to determine the critical particle diameters for activation with a method similar to that introduced in Wex et al. (2007).

Based on this closure, a new parameterization to consistently describe sea-salt-particle hygroscopic growth (at RH>95 %) and activation was developed.

2 Chemical composition of the sea-water samples

Three different sea-water samples were analyzed with respect to hygroscopic growth and activation. Two samples came from the Baltic Sea, sample I from the bay of Mecklenburg (54°18.90′ N; 11°33.00′ E) and sample II from east of Gotland (57°19.20′ N; 20°03.00′ E), both were collected in a depth of about 1–2 m. Sample III was taken from the Atlantic Ocean (only the sample latitude of 45° N is known) in a depth of 3000 m.

The three sea-water samples were analyzed concerning their inorganic chemical composition. The samples for analysis of main ions were filtered and analyzed by ion chromatography (IC, Metrohm-Switzerland). A detailed description is given by Brüggemann and Rolle (1998). The concentrations C_s (g·l^{-1}) and the mass fractions ξ_s (%) of the detected ions are shown in Table 1. Besides these, more ions were found in the different samples in marginal concentrations (lower than the concentrations of the NO_3^--ions). The salinities of the Baltic sea samples were lower (8.16 g·l^{-1} for sample I and 7.18 g·l^{-1} for sample II) than the salinity of the Atlantic sample (31.73 g·l^{-1}). Cl$^-$

and Na$^+$ are the major ions for all samples. Regarding the mass fractions, the Atlantic sample and the two Baltic Sea samples differ in these two main ions only. While the fraction of the Cl$^-$ ions in the Atlantic sample is higher compared to the two Baltic Sea samples, the fraction of the Na$^+$ ions is lower compared to both Baltic Sea samples.

5   Based on the knowledge of the mass fraction and the molecular weight of the ions, for each sea-water sample the analyzed ions are combined to salts, which can be found in sea-salt particles: NaCl, MgCl$_2$, MgSO$_4$, Na$_2$SO$_4$, CaCl$_2$ and KNO$_3$. The analysis of the pH value showed that each sea-water sample was nearly neutral. Therefore no compensation with H$^+$ and OH$^-$ ions had to be taken into account. The concentrations

10 and the mass fractions of these salts are shown in Table 2 for each sea-water sample. With this knowledge and the mass fraction mixing rule the mean density ρ_s and mean molecular weight M_s were calculated of the particles which were generated from these sea-water samples:

$$\text{Sample I} \quad \rho_s = 2245.9 \text{ kg·m}^{-3} \quad M_s = 67.7 \text{ g·mol}^{-1}$$
$$\text{Sample II} \quad \rho_s = 2248.7 \text{ kg·m}^{-3} \quad M_s = 68.4 \text{ g·mol}^{-1}$$
$$\text{Sample III} \quad \rho_s = 2238.4 \text{ kg·m}^{-3} \quad M_s = 67.6 \text{ g·mol}^{-1}.$$

These values have to be considered as an approximation because of the assump-

15 tions that were used in their derivation. But the influence of NaCl in the sea-water samples can already be seen.

3   Experimental setup

Figure 1 shows the experimental setup. The sea-salt particles were generated from the three sea-water samples by using an atomizer (TSI 3075, TSI Inc., St. Paul, Minnesota,

20 USA). NaCl-particles were used as a reference throughout the whole work. All particles were generated by atomizing aqueous solutions of 2 g salt (the sea-water samples were diluted accordingly) per liter of double de-ionized water.

The resulting aerosol particles were dried in a diffusion dryer. A DMA (Differential Mobility Analyzer, Knutson and Whitby (1975), type "Vienna medium") was used to select a narrow dry particle size fraction. For hygroscopic growth measurements the investigated mobility diameters of the selected dry particles were 150 and 200 nm for the three sea-salt samples and NaCl. During the activation measurements, the dry mobility diameters were varied for fixed supersaturations.

The cubical shape of NaCl particles had to be accounted for by using a shape factor of 1.08 (Kelly and McMurry, 1992). As NaCl is the main component of the sea-salt particles, it could not be excluded that sea-salt particles require a shape factor, too for their description. Investigations with a system consisting of a DMA and an ELPI (Electric Low Pressure Impactor, Fernández de la Mora et al., 1990) showed that the NaCl particles and the particles from the three different sea-salt samples possess the same aerodynamic behavior and therefore the same shape factor (see Appendix). Hence, for the investigations a shape factor of 1.08 was used for all sea-salt particles. From this it follows that the mass equivalent diameters of the selected particles were 139 nm and 185 nm for the hygroscopic growth measurements.

The number concentrations of the selected particles were determined with a CPC (TSI 3010, TSI Inc., St. Paul, Minnesota, USA), and were kept at 300–500 cm^{-3} with a dilution system upstream of the DMA. All flows were controlled with mass flow controllers (MKS 1179, MKS Instruments Deutschland GmbH, München, Germany) and were checked on a daily basis with a bubble flow meter (Gilian$^®$ Gilibrator^{TM}2, Sensidyne Inc., Clearwater, Florida, USA).

Before entering LACIS, the aerosol passed through a saturator (Perma Pure MH-110-12S-4, Perma Pure LLC, Toms River, New Jersey, USA). The saturator consisted of a tube made of Nafion$^®$ which was surrounded by temperature-controlled water. The temperature of the water-jacket was kept at a defined value by circulating the water through a thermostat (HAAKE C25P, HAAKE GmbH, Karlsruhe, Germany). The temperature of the thermostat was regulated by the signal of a Pt-100 resistance thermometer that measured the temperature of the water at the aerosol outlet of the satu-

rator. Therewith, the saturator was used in a counter flow fashion. Downstream of the saturator, the dew point temperature of the aerosol was equal to the temperature at the saturator outlet. This was verified with a dew point mirror (Dew Prime I-S2, Edge Tech, Milford, Massachusetts, USA), which measures with an accuracy of 0.1 K. A similar setup was used to humidify particle-free sheath air. Humidified aerosol and sheath air, both with the same dew point temperatures, were combined in the LACIS head. The aerosol was confined by the sheath air in a narrow beam (about 2 mm in diameter) at the center axis of LACIS.

LACIS itself is a laminar flow tube with a diameter of 15 mm and a length of 1 m, surrounded by a thermostated water-jacket (thermostat: HAAKE C40P, HAAKE GmbH, Karlsruhe, Germany). The difference between the dew point temperature of the aerosol and sheath air flow and the temperature of the LACIS water-jacket determines the RH inside LACIS. For studying the hygroscopic growth of the different salt particles, LACIS was kept at a constant temperature of 20.0°C. The saturator temperatures were varied from 16.5°C to 19.9°C, resulting in relative humidities (RH) from 79.8% to 98.8%. Inside the flow tube, the RH reaches a constant value at approximately 20 cm downstream of the inlet. When measuring particle activation, the saturator temperature was kept at a constant temperature of 22.0°C. The temperature of the LACIS water-jacket was set to different temperatures: 5.65°C, 5.45°C and 5.3°C. This is equivalent to supersaturations of 0.10%, 0.16% and 0.30%.

The residence time of the aerosol inside LACIS is about 2 s. At the outlet of the flow tube the size of the grown particles/droplets is measured with an optical particle counter (OPC) that was designed and built especially for LACIS. For a detailed description see Kiselev et al. (2005). The optical particle sizer was calibrated with PSL particles with diameters of 299 nm, 404 nm, 499 nm, 701 nm, 799 nm and 1444 nm. For the determination of the response function of the OPC, the refractive index of the humidified particles, which varies as a particle grows, was estimated using a volume mixing rule (e.g., Seinfeld and Pandis, 1998).

EGU

4   Theory

For the simulation of the measured hygroscopic growth simple Köhler theory, including the Kelvin- and the Raoult-term, was applied (Pruppacher and Klett, 1997):

$$S = \exp\left(\frac{4M_w\sigma_{sol}}{RT\rho_w D_{wet}} - \frac{\frac{\nu\phi_s\rho_s}{M_s}V_s M_w}{m_w}\right). \tag{1}$$

5 with the saturation S, the molecular weight of water M_w and the solute M_s, the water mass m_w, the solute Volume V_s, the density of water ρ_w and the solute ρ_s, the osmotic coefficient ϕ_s (accounting for the non-ideality of the solution), the number of ions ν per solute molecule, the surface tension of the solution σ_{sol}, the gas constant R, the temperature T and the droplet diameter D_{wet}.

10   For this study, the surface tension of water σ_w is used in the Kelvin-term of the Köhler theory.

In the Raoult-term, neither ϕ_s nor ν are known, and for ρ_s and M_s only the approximations derived in Sect. 2 exist for the different sea-salt samples. Therefore these parameters are combined into a so called "ionic density" ρ_{ion} (unit: mol·m^{-3}) (Wex
15 et al., 2007):

$$\rho_{ion} = \frac{\nu\phi_s\rho_s}{M_s}. \tag{2}$$

ρ_{ion} is derived for each sea-salt sample using the measured hygroscopic growth and is later on used to determine critical diameters for the activation for the CCN-closure, performed in this study.

EGU

5 Measurements of hygroscopic growth and activation of the sea-salt particles

5.1 Hygroscopic growth

The measurements were performed for RHs between 79.8% and 98.8%. The used RH-range was calibrated with ammonium sulfate particles. In Fig. 2, RHs as determined from the hygroscopic growth of NaCl particles with a dry mass equivalent diameter D_{me_0} of 189 nm are plotted versus RHs resulting from the calibration with ammonium sulfate particles with D_{me_0}=200 nm. For both materials Köhler theory with ϕ_s according to Pruppacher and Klett (1997) and the surface tension of water were used. For RH>86%, the quality of the calibration becomes clear, as the maximum relative deviation amounts to 0.5%.

For the investigations of the sea-salt and NaCl particles, mass-equivalent particle diameters of 139 nm and 185 nm were used. For each RH, each substance and each particle diameter at least three measurements were performed.

As an example Fig. 3 shows the hygroscopic growth of the sea-salt particles for sample III. Plotted are wet diameters D_{wet} as function of RH for the two dry diameters considered. In addition results for the NaCl particles are given. The data points represent the mean values of at least three independent measurements. The error bars, being a measure for the experimental uncertainties, represent the maximum deviation from the mean values. These uncertainties also include the influences of fluctuations in RH. Due to the lower detection limit of the OPC used to determine the size of the grown droplets, for salt particles with a dry diameter of 139 nm only RHs larger than 84% were considered.

From Fig. 3 it can be seen, that especially at high RHs, the sea-salt particles exhibit a reduced growth compared to the NaCl particles. Similar behavior was observed for all three sea-water samples, i.e., also for the two Baltic sea-water samples. In Fig. 4 the hygroscopic growth of the three samples is shown for a dry particle diameter of 185 nm in comparison to NaCl particles with the same dry size. The measured grown sizes for particles generated from the three sea-water samples agree within the experimental

EGU

uncertainties. This was also found for the dry diameter of 139 nm. In other words, the hygroscopic growth of the three sea-water was found to be very similar but always lower than that of the pure NaCl particles.

5.2   Activation

Measurements were performed at supersaturations of 0.10%, 0.16% and 0.30%. The calibration of LACIS with respect to the supersaturation was done with ammonium sulfate particles (Wex et al., 2006). At each supersaturation the diameter of the investigated dry salt particles was varied until the critical diameter D_{crit} was found. D_{crit} is the diameter where the saturation in LACIS corresponded to the critical supersaturation which the particles needed to activate to cloud droplets. As for the investigations of hygroscopic growth, each activation measurement was repeated at least two times to gain a measure for the measurement uncertainties.

Figures 5 and 6 depict droplet diameters as measured for sea-salt (sample III) and NaCl particles, respectively as function of dry particle size. Values for the three different supersaturations are given. The data points represent mean values of at least two measurements which were performed on different days. The errors bars represent the maximum deviation from the mean values. The particles for which the supersaturation in LACIS is not sufficient for activation grow hygroscopically. They are in equilibrium with their environment. The larger particles for which the present saturation in LACIS is adequate for activation grow dynamically. Earlier activation measurements (Wex et al., 2006) showed that the results for hygroscopically grown particles could be linked through a straight line. The results for dynamically grown particles, however, could be reproduced by a polynomial curve. The intercept point of the polynomial curve and the straight line indicates D_{crit}.

In Table 3, values of D_{crit} are given for all sea-salt samples and for NaCl. The given critical diameters correspond to the mean values of at least two measurements. The uncertainties represent the maximum deviation from the mean values found. It should be noted, that earlier calibrations regarding the supersaturations (and the correspond-

ing uncertainties) inside LACIS yielded an uncertainty of approximately ±0.03% in the supersaturation range used in this study.

At 0.10% supersaturation, the measured critical diameters for all sea-salt samples and for pure NaCl are identical within the measurement uncertainties. This is similar for the measurements at 0.16%, where D_{crit} of all sea-salt samples is slightly larger than that of NaCl. At 0.30%, D_{crit} of the sea-salt samples also is larger than that of NaCl, even exceeding the measurement uncertainty for sample I.

In summary, the activation behavior found for particles generated from the three sea-salt samples and from NaCl are nearly identical.

6 CCN-closure

The concept of ρ_{ion} (Wex et al., 2007) was utilized to carry out a CCN closure test and to develop a parameterization for a consistent description of sea-salt particle hygroscopic growth and activation.

6.1 Obtaining ρ_{ion} from the measured hygroscopic growth

Köhler theory as described in Sect. 4 was used to simulate the measured hygroscopic growth of the different sea-salts and the NaCl particles. In the Köhler model, ρ_{ion} was varied until the calculated wet diameters agreed with the measured values. This procedure was performed separately for each RH at which the measurements were performed.

The resulting values for ρ_{ion} together with the calculated values of the density and the molecular weight of the three sea-salts can be used to derive the product of osmotic coefficient ϕ_s and the number of the dissociated ions v per molecule for each sea-salt. In Fig. 7, this product is plotted versus the molality for the three sea-salts and NaCl. The theoretical curve for NaCl (Pruppacher and Klett, 1997) is shown as well. The

[EGU]

corresponding molality M is computed from:

$$M = \frac{D_{me_0}^3}{D_{wet}^3 - D_{me_0}^3} \frac{\rho_s}{M_s \rho_w} \tag{3}$$

The calculations are based on the hygroscopic growth data of the particles with a dry diameter of 189 nm. The uncertainties result from the maximum deviations as given with the examples in Fig. 3. It is obvious that the three samples and NaCl lie close to the theoretical curve for NaCl (see Fig. 7). The maximum deviation from the theory amounts to 11%. The trend of the product $\phi_s \nu$ as given in Pruppacher and Klett (1997) for NaCl was reproduced for all sea-salt samples, implying a similar tendency with respect to non-ideal behavior, which is probably determined by the main compound NaCl.

For the calculation of the critical diameters, i.e., the diameters at which particles activate to become cloud droplets, only values of ρ_{ion} for RHs above 95% were considered. In this RH range, which corresponds to molalities smaller than 1.5 mol·kg^{-1} here, ρ_{ion} is nearly constant and can be assumed to be a good approximation for the ρ_{ion} at the point of activation. In Fig. 8, the average values for ρ_{ion} in the RH range >95% are shown for the three sea-salt samples and pure NaCl.

A dilute solution of NaCl in water behaves nearly ideally ($\phi_s \approx 1, \nu = 2$), and the density and molecular weight of NaCl are known. Thus, a theoretical value for ρ_{ion} can be calculated. This value is presented in Fig. 8, too (open square). It is obvious that this value lies well within the uncertainty of the experimentally determined ρ_{ion}. This underlines the high quality of the determined ionic densities and the feasibility and quality of the parameterization concept based on ρ_{ion}.

6.2 Comparison of the calculated and measured critical diameters

The derived values of ρ_{ion} were used in the Köhler equation to calculate the critical diameters. The calculations were done for the three supersaturations: 0.10%, 0.16%

and 0.30% considered during the experiments. In Fig. 9 the calculated and measured values of D_{crit} are shown.

For the supersaturation of 0.10% the measured values of D_{crit} of NaCl, sample I, II and III are 4%, 4.3%, 4.3% and 10.3% smaller than the calculated ones. Apart from sample III the measured and calculated critical diameters agree within the uncertainties. The measured and calculated critical particle diameters coincide within the measuring accuracy at the supersaturation of 0.16% for all four substances. The measured value for NaCl is 0.6% higher than the calculated diameter. The measured diameters for sample II and III are 3.9% and 3.3% smaller than the calculated value. The measured and the calculated D_{crit} coincide for sample I. At the supersaturation of 0.30%, the measured values of D_{crit} of NaCl, sample II and III are 4.2%, 6.5% and 2.9% below the calculated ones. The measured value of sample I lies 4.4% above the measured diameter. Except for sample II the measured and calculated values agree within the uncertainties. The suboptimal agreement between calculation and measurement for sample III at 0.10% and sample II at 0.30% supersaturation might result from uncertainties of the supersaturation inside LACIS. This uncertainty is approximately ± 0.03% which explains the discrepancies found as the considered particle diameters of 99 nm for sample III and 49 nm for sample II require critical supersaturation of 0.12% and 0.33%, respectively.

In summary, using Köhler theory and ρ_{ion} as determined from hygroscopic growth measurements, the critical diameters and consequently critical supersaturations at which particles activate to cloud droplets, were determined with good accuracy. The activation behavior of the three sea-salt-samples and NaCl was found to be nearly identical. Based on this, a new parameterization

$$S = \exp\left(\frac{4 M_w \sigma_w}{RT \rho_w D_{wet}} - \rho_{ion} \frac{M_w}{\rho_w} \frac{D_{me_0}^3}{D_{wet}^3 - D_{me_0}^3}\right) \qquad (4)$$

|◄ | ►|

◄ | ►

Back | Close

Full Screen / Esc

Printer-friendly Version

Interactive Discussion

EGU

respectively in linearized form (just given here for convenience)

$$S = 1 + \frac{4M_w\sigma_w}{RT\rho_w D_{\text{wet}}} - \rho_{\text{ion}}\frac{M_w}{\rho_w}\frac{D_{me_0}^3}{D_{\text{wet}}^3 - D_{me_0}^3} \qquad (5)$$

has been developed, to describe consistently sea-salt-particle hygroscopic growth (at RH>95%) and activation. The parameterization is based on the concept of ρ_{ion} (Wex et al., 2007) and the assumption of a surface tension equal to that of water ($\sigma_w = 72.8\,\text{mN·m}^{-1}$) at activation. For sea-salt, a mean value of $62\,500\,\text{mol·m}^{-3}$ for ρ_{ion} can be used. Entering these values of ρ_{ion}, σ_w and the other known parameters ($\rho_w = 997\,\text{kg·m}^{-3}$, $M_w = 0.018\,\text{kg·mol}^{-1}$ and $R = 8.314\,\text{J·K}^{-1}\text{·mol}^{-1}$) in Eq. (5), it follows:

$$S = 1 + \frac{6.32 \times 10^{-7}}{T}\frac{1}{D_{\text{wet}}} - 1.13\frac{D_{me_0}^3}{D_{\text{wet}}^3 - D_{me_0}^3}. \qquad (6)$$

7 Conclusions

The hygroscopic growth of sea-salt particles generated from three different sea-water samples was investigated with LACIS at RHs from 79.8% up to 98.8%. For comparison the growth of pure NaCl particles was considered, as well. The cubical shape of the NaCl particles was accounted for by using the shape factor of 1.08. Additionally, electrical low pressure impactor measurements showed that sea-salt particles exhibit an aerodynamic behavior similar to that of NaCl particles. Consequently, the shape factor of 1.08 was used when converting from mobility to mass equivalent diameter.

The measurements showed that the hygroscopic growth of the three different sea-salt particles for the dry particle diameters of 139 nm and 185 nm agrees within the measurement uncertainties. The marginal differences in the chemical composition did not result in visible differences in the hygroscopic growth. The hygroscopicity of the three sea-water samples was always lower than that of the pure NaCl particles with the

same dry sizes. This suggests that the existence of additional material in the sea-salt particles reduces the hygroscopic growth slightly in comparison to pure NaCl particles.

The activation of the sea-salt particles was investigated for the supersaturations 0.10%, 0.16%, and 0.30%. The critical diameters D_{crit} of the three sea-salt samples agree within the measurements uncertainties. As found in the hygroscopicity measurements, marginal differences in the chemical composition between the three sea-water samples caused no significant difference in the activation behavior. Additionally, the measured D_{crit} of the sea-salt particles agree with those of pure NaCl within the measurement uncertainties for all supersaturations investigated.

For the first time, CCN-closure was tested for sea-salt particles. For that purpose, hygroscopic growth data and simple Köhler theory were used to derive critical diameters which activated at the adjusted supersaturations for each sea-salt sample. For the closure, a mean value of ρ_{ion} for each sample was determined based on measured hygroscopic growth at RHs between 95% and 98.8%. With the derived values of ρ_{ion}, and assuming the surface tension of water, values of D_{crit} were calculated. Measured and calculated values of D_{crit} agree within the uncertainties and consequently, CCN-closure was performed successfully.

Based on the successful closure, a new parameterization to consistently describe sea-salt-particle hygroscopic growth (at RH>95 %) and activation has been developed.

Appendix A

It is well-known that dry NaCl particles possess a cubical shape. With the DMA selected mobility diameter D_{mob} is not equal to the mass equivalent diameter D_{me}. Therefore D_{mob} has to be shape corrected (Kelly and McMurry, 1992; Gysel et al., 2002).

Since the main compound of the three different sea-salt samples is NaCl, it is important to know if the generated sea-salt particles possess a shape factor, too. For the detection, a system consisting of a DMA and an ELPI (Electrical Low Pressure Impactor, Fernández de la Mora et al., 1990) is used (see Fig. A1). The ELPI operates

Sea-salt particle hygroscopic growth and activation

D. Niedermeier et al.

in the free-molecular regime, i.e., the mean free path of the molecules is significantly larger than the particle sizes. Therefore the retrieved particle diameter is the vacuum-aerodynamic diameter D_{va}.

For the investigations, the sea-salt particles were generated from the three different sea-water samples by using an atomizer. As reference NaCl particles were generated by atomizing an aqueous salt solution.

The resulting aerosol particles were dried in a diffusion dryer. A DMA was used to select several dry mobility diameters. One part of the selected quasi monodisperse aerosol was led into the CPC while the other was directed into the ELPI.

The impaction behavior is normally described by the Stokes-number Stk. For the ELPI Stk is written as (Fernández de la Mora et al., 1990):

$$Stk = \frac{0.178\dot{m}c_0^3}{8h^3} \cdot \rho_p D_{me} \cdot \frac{1}{p^2} = \frac{l_{stop}}{h}, \tag{A1}$$

where $\dot{m}$ is the gas mass flow through the impactor nozzle, c_0 is the sonic speed, $2h$ is the diameter of the impactor nozzle. Furthermore ρ_p and D_{me} are the bulk density and the mass equivalent diameter of the particles and p is the impact pressure in the ELPI chamber.

If the Stokes-number exceeds a critical value, the particles with one D_{va} are deposited on the impactor plate. The pressure, where 50% of the particles with equal D_{va} are deposited on the plate, is defined as the impaction pressure p_{50}. The connection between D_{va} (respectively D_{me}) and p_{50} is:

$$\rho_0 \cdot D_{va} = \rho_p \cdot \frac{D_{me}}{\chi_v} = k_1 \cdot p_{50}^2 + k_2, \tag{A2}$$

where χ_v is the shape factor of the free molecular regime and k_1 and k_2 are two constants which will be detected in the following. Replacing D_{me} in Eq. (A2) through

EGU

$D_{me} = \frac{D_{mob}}{\chi_c} \frac{C_c(D_{me})}{C_c(D_{mob})}$ (see DeCarlo et al., 2004) yields:

$$\rho_p \cdot D_{mob} = \chi_v \chi_c \frac{C_c(D_{mob})}{C_c(D_{me})} \left(k_1 p_{50}^2 + k_2 \right) , \qquad (A3)$$

where χ_c is the shape factor in the continuum regime. C_c is the slip correction. The constants k_1 and k_2 were determined with Polystyrol-Latex (PSL) particles. For several D_{mob} the corresponding impaction pressure p_{50} values were determined. In Fig. A2, the product $\rho_p D_{mob}$ is plotted against p_{50}^2 for the PSL particles. Since $\chi_v = \chi_c = 1$, $D_{mob} = D_{me}$ and ρ_p is known for these particles, k_1 and k_2 can be determined from the slope and the location of the linear regression line.

For the NaCl and sea-salt particles, the values of p_{50} were determined for several D_{mob}, as well. For ρ_p of the different sea-salt samples, the values listed in Sect. 2 were used. In Fig. A2, the product $\rho_p D_{mob}$ is also plotted against p_{50}^2 for the NaCl and the sample I particles exemplarily (The data points of sample II and III are nearly identical to sample I). The collected data points were approximated by a linear regression.

It is obvious that the NaCl and sea-salt particles possess a similar aerodynamic behavior. So the product: $\chi_v \chi_c \frac{C_c(D_{mob})}{C_c(D_{me})}$ is nearly identical for the NaCl and the sea-salt particles (the difference between the shape factors is about 0.003, i.e. negligible). Therefore the shape factor of 1.08 was used for the sea-salt particles.

References

Andreae, M. O. and Raemdonck, H.: Dimethyl sulfide in the surface ocean and the marine atmosphere: A global view, Science, 221, 744–747, 1983. 11513

Andreae, M. O., Ferek, R. J., Bermond, F., Byrd, K. P., Engstrom, R. T., Hardin, S., Houmere, P. D., LeMarrec, F., Raemdonck, H., and Chatfield, R. B.: Dimethyl sulfide in the marine atmosphere, J. Geophy. Res., 999, 12 891–12 900, 1985. 11513

Blanchard, D. C. and Cipriano, R. J.: Biological regulation of climate, Nature, 330, 526, 1987. 11514

Sea-salt particle hygroscopic growth and activation

D. Niedermeier et al.

EGU

Blanchard, D. C. and Woodcock, A. H.: Bubble formation and modification in the sea and its meteorological significance, Tellus, 9, 145–158, 1957. 11513

Blanchard, D. C. and Woodcock, A. H.: The production, concentration, and vertical distribution of the sea-salt aerosol, The New York Academy of Sciences, 338, 330–347, 1980. 11513

5 Brüggemann, E. and Rolle, W.: Changes of some components of precipitation in East Germany after the unification, Water Air and Soil. Pollut. 107, 1–23, 1998. 11515

Charlson, R. J., Lovelock, J. E., Andreae, M. O., and Warren, S. G.: Oceanic phytoplankton, atmospheric sulfur, cloud albedo and climate, Nature, 326, 655–661, 1987. 11513

DeCarlo, P. F., Slowik, J. G., Worsnop, D. R., Davidovits, P., and Jimenez, J. L.: Particle mor-
10 phology and density characterization by combined mobility and aerodynamic measurements. Part 1: Theory, Aerosol Sci. Technol., 38, 1185–1205, 2004. 11528

Fernández de la Mora, J., Rao, N., and McMurry, P. H.: Inertial impaction of fine particles at moderate reynolds numbers and in the transonic regime with a thin-plate orifice nozzle, J. Aerosol Sci., 21, 889–909, 1990. 11517, 11526, 11527

15 Fitzgerald, J. W.: Marine Aerosol: A Review, Atmos. Environ., 25A, 533–545, 1991. 11512, 11513

Gong, S. L., Barrie, L. A., and Blanchet, J.-P.: Modeling sea-salt aerosols in the atmosphere 1. Model development, J. Geophy. Res., 102, 3805–3818, 1997. 11513

Gysel, M., Weingartner, E., and Baltensperger, U.: Hygroscopicity of aerosol particles at low
20 temperatures. 2. Theoretical and experimental hygroskopic properties of laboratory gener-ated aerosols, Environ. Sci. Technol., 36, 63–68, 2002. 11526

Hudson, J. G. and Frisbie, P. R.: Cloud condensation nuclei near marine stratus, J. Geophy. Res., 96, 20 795–20 808, 1991. 11515

Kelly, W. P. and McMurry, P. H.: Measurement of particle density by inertial classification of
25 differential mobility analyzer-generated monodisperse aerosols, Aerosol Sci. Technol., 17, 199–212, 1992. 11517, 11526

Kiselev, A., Wex, H., Stratmann, F., Nadeev, A., and Karpushenko, D.: White-light optical par-ticle spectrometer for in situ measurements of condensational growth of aerosol particles, Appl. Opt., 44, 4693–4701, 2005. 11518

30 Knutson, E. O. and Whitby, K. T.: Aerosol classification by electronic mobility: Apparatus, the-ory, and applications, J. Aerosol Sci., 6, 443–451, 1975. 11517

Leck, C. and Bigg, E. K.: Evolution of the marine aerosol - A new perspective, Geophys. Res. Lett., 32, doi:10.1029/2005GL023651, 2005. 11513

Sea-salt particle hygroscopic growth and activation

D. Niedermeier et al.

Title Page

Abstract	Introduction
Conclusions	References
Tables	Figures

◄◄   ►►

◄   ►

Back   Close

Full Screen / Esc

Printer-friendly Version

Interactive Discussion

EGU

Leck, C. and Bigg, E. K.: Biogenic particles in the surface microlayer and overlaying atmosphere in the central Artic Ocean during summer, Tellus, 57B, 305–316, 2005. 11513

O'Dowd, C. D. and Smith, M. H.: Physicochemical properties of aerosols over the northeast atlantic: Evidence for wind-speed-related submicron sea-salt aerosol production, J. Geophy. Res., 98, 1137–1149, 1993. 11513

O'Dowd, C. D., Smith, M. H., Consterdine, I. E., and Lowe, J. A.: Marine aerosol, sea-salt, and the marine sulphur cycle: A short review, Atmos. Environ., 31, 73–80, 1997. 11513, 11514

Pilinis, C., Pandis, S. N., and Seinfeld, J. H.: Sensitivity of direct climate forcing by atmospheric aerosols to aerosl size and composition, J. Geophy. Res., 100, 18 739–18 754, 1995. 11512

Pruppacher, H. R. and Klett, J. D.: Microphysics of Clouds and Precipitation, Kluwer Academic Publishers, Dordrecht, The Netherlands, 1997. 11519, 11520, 11522, 11523

Randall, D. A., Coakley, J. A., Fairall, C. W., Kropfli, R. A., and Lenschow, D. H.: Outlook for research on subtropical marine stratiform clouds, Bull. Amer. Meteor. Soc., 65, 1290–1301, 1984. 11513

Randles, C. A., Russell, L. M., and Ramaswamy, V.: Hygroscopic and optical properties of organic sea salt aerosol and consequences for climate forcing, Geophy. Res. Lett., 31, L16108, doi:10.1029/2004GL020628, 2004. 11512

Seinfeld, J. H. and Pandis, S. N.: Atmospheric chemistry and physics: From air pollution to climate change, Wiley-Interscience Publication, Wiley, New York, 1998. 11518

Stratmann, F., Kiselev, A., Wurzler, S., Wendisch, M., Heintzenberg, J., Charlson, R. J., Diehl, K., Wex, H., and Schmidt, S.: Laboratory Studies and Numerical Simulations of Cloud Droplet Formation under Realistic Supersaturation Conditions, J. Atmos. Ocean. Technol., 21, 876–887, 2004. 11514

Wex, H., Kiselev, A., Stratmann, F., and Zoboki, J.: Measured and modeled equilibrium sizes of NaCl and $(NH_4)_2SO_2$ at relative humidities up to 99,1%, J. Geophy. Res., 110, D21212, doi:10.1029/JD005507, 2005. 11514

Wex, H., Kiselev, A., Ziese, M., and Stratmann, F.: Calibration of LACIS as a CCN detector and its use in measuring activation and hygroscopic growth of atmospheric aerosl particles, Atmos. Chem. Phys., 6, 4519–4527, 2006,
http://www.atmos-chem-phys.net/6/4519/2006/. 11521

Wex, H., Kiselev, A., Stratmann, F., and Zoboki, J.: A CCN-closure-study for HULIS Aerosol, Geophy. Res. Lett., 34, L02818, doi:10.1029/2006GL028260, 2007. 11515, 11519, 11522, 11525

Sea-salt particle hygroscopic growth and activation

D. Niedermeier et al.

Title Page

Abstract	Introduction
Conclusions	References
Tables	Figures

◀◀   ▶▶

◀   ▶

Back   Close

Full Screen / Esc

Printer-friendly Version

Interactive Discussion

EGU

Table 1. Concentration and mass fraction of major ions for the three sea-water samples.

Ions	Sample I C_s [g·l^{-1}]	ξ_s [%]	Sample II C_s [g·l^{-1}]	ξ_s [%]	Sample III C_s [g·l^{-1}]	ξ_s [%]
Cl^-	4.22	51.75	3.87	53.94	19.37	61.06
NO_3^-	0.02	0.25	0.04	0.56	0.05	0.14
SO_4^{2-}	0.75	9.17	0.56	7.85	2.82	8.89
Na^+	2.60	31.89	2.18	30.39	7.66	24.15
K^+	0.13	1.59	0.09	0.09	0.36	1.12
Mg^{2+}	0.25	3.04	0.29	3.97	1.08	3.41
Ca^{2+}	0.19	2.31	0.15	2.06	0.39	0.39

EGU

EGU

Table 2. Concentration and mass fraction of the possible salts for the three sea-water samples.

Salt	Sample I C_s [g·l^{-1}]	ξ_s [%]	Sample II C_s [g·l^{-1}]	ξ_s [%]	Sample III C_s [g·l^{-1}]	ξ_s [%]
NaCl	5.88	73.56	4.95	69.99	18.28	70.74
MgCl$_2$	0.63	7.83	0.96	13.51	4.23	16.38
Na$_2$SO$_4$	0.89	11.18	0.72	10.16	1.45	5.60
CaCl$_2$	0.30	3.74	0.24	3.44	1.08	4.18
KNO$_3$	0.03	0.41	0.07	0.92	0.07	0.28
K$_2$SO$_4$	0.26	3.28	0.14	1.98	0.73	2.82

EGU

Table 3. Measured critical diameters and their experimental uncertainties for the three sea-salt samples and NaCl.

S %	Sample I [nm]	Sample II [nm]	Sample III [nm]	NaCl [nm]
0.10	105.0±5.0	105.0±4.0	99.0±5.0	100.0±4.0
0.16	80.0±3.0	77.0±3.0	77.0±3.0	76.5±3.0
0.30	55.0±2.0	49.5±2.0	51.0±2.0	48.0±2.0
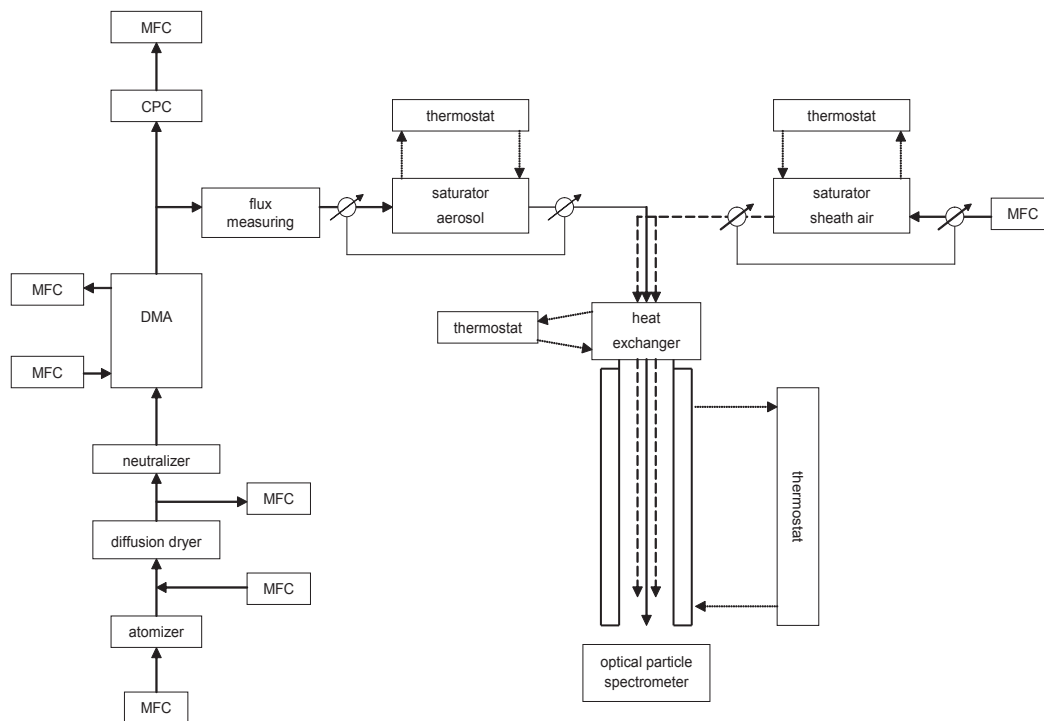
Fig. 1. Set-up of the particle generation and the LACIS flow tube.

EGU
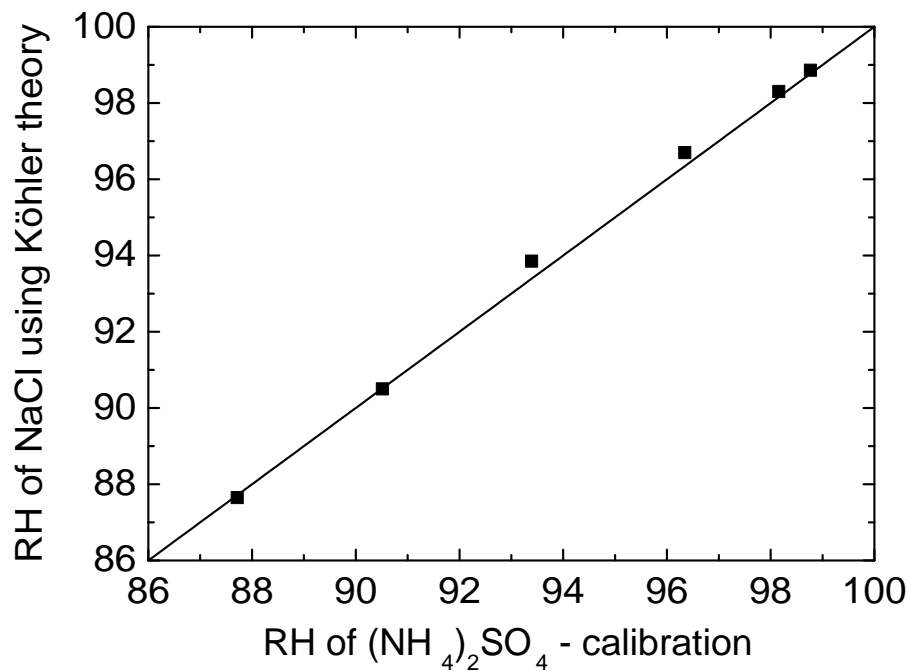
Fig. 2. RHs as determined from the hygroscopic growth of NaCl particles with D_{me_0} = 189 nm are plotted versus RHs resulting from the calibration with ammonium sulfate particles with D_{me_0} = 200 nm.
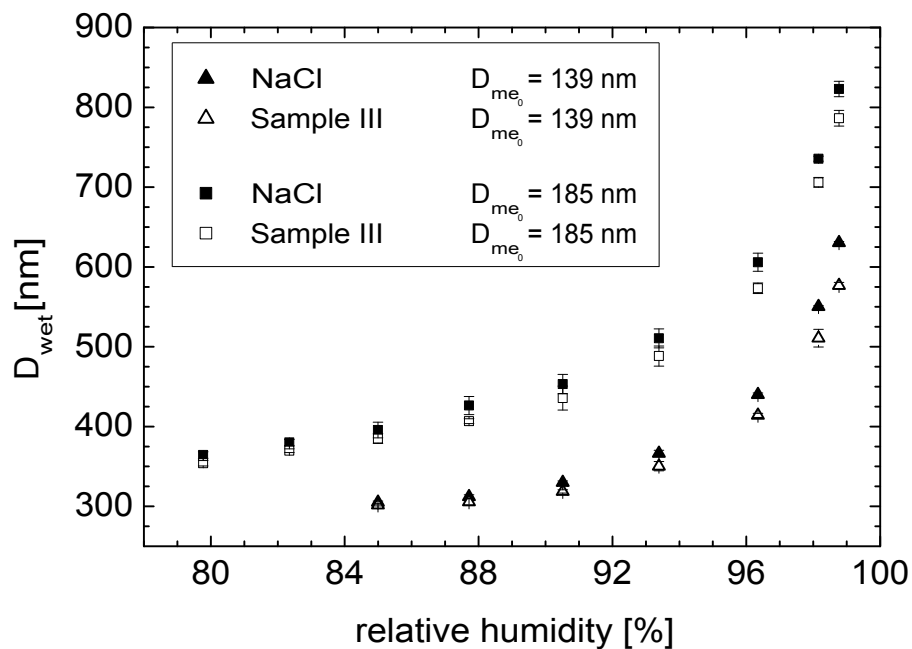
Fig. 3. Hygroscopic growth of the sea-salt particles of sample III at different values of RH compared to that of pure NaCl.

EGU

EGU
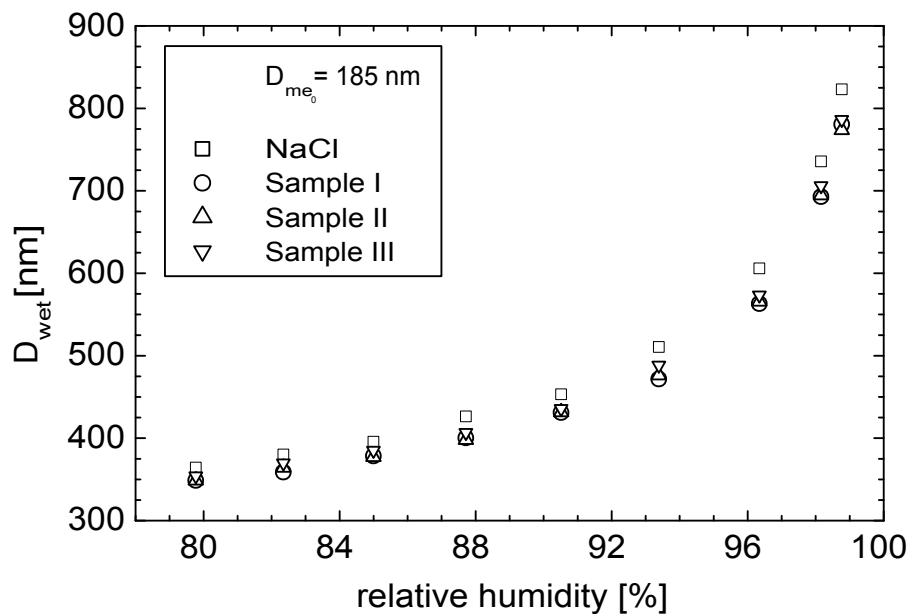
Fig. 4. Hygroscopic growth of sea-salt particles of the three different samples at different values of RH in comparison to pure NaCl.
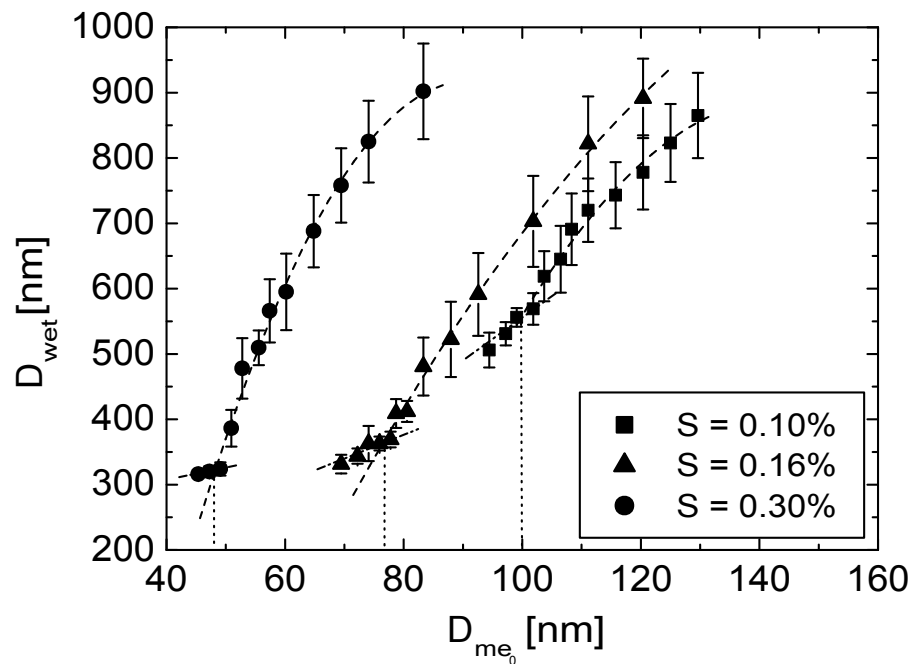
Fig. 5. Activation curves of the sea-salt particles of sample III at three different supersaturations.

Title Page

Abstract | Introduction

Conclusions | References

Tables | Figures

◀ | ▶|

◀ | ▶

Back | Close

Full Screen / Esc

Printer-friendly Version

Interactive Discussion

EGU

EGU
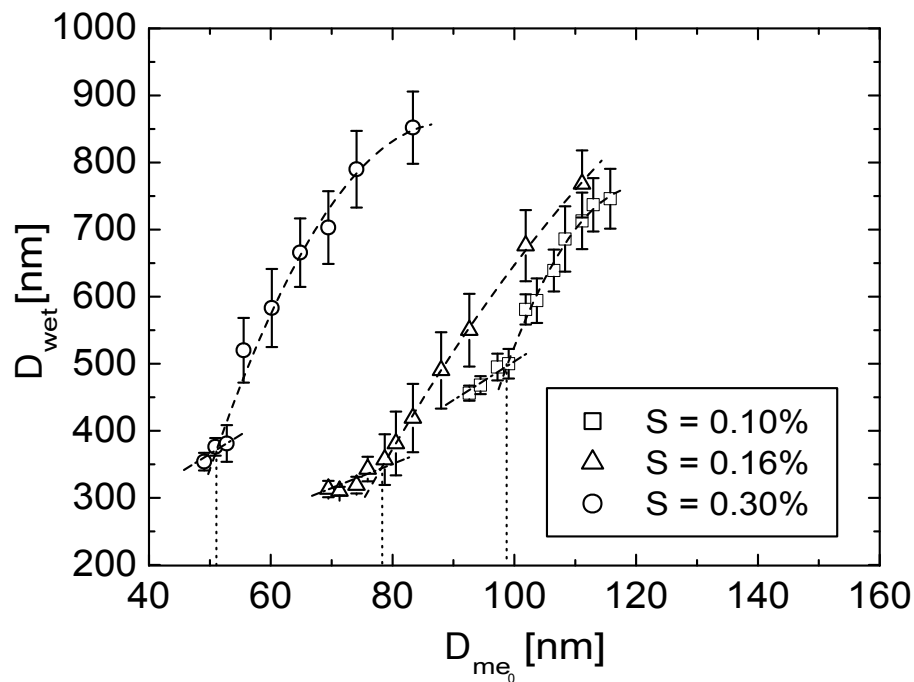
Fig. 6. Activation curves of the NaCl particles at three different supersaturations.
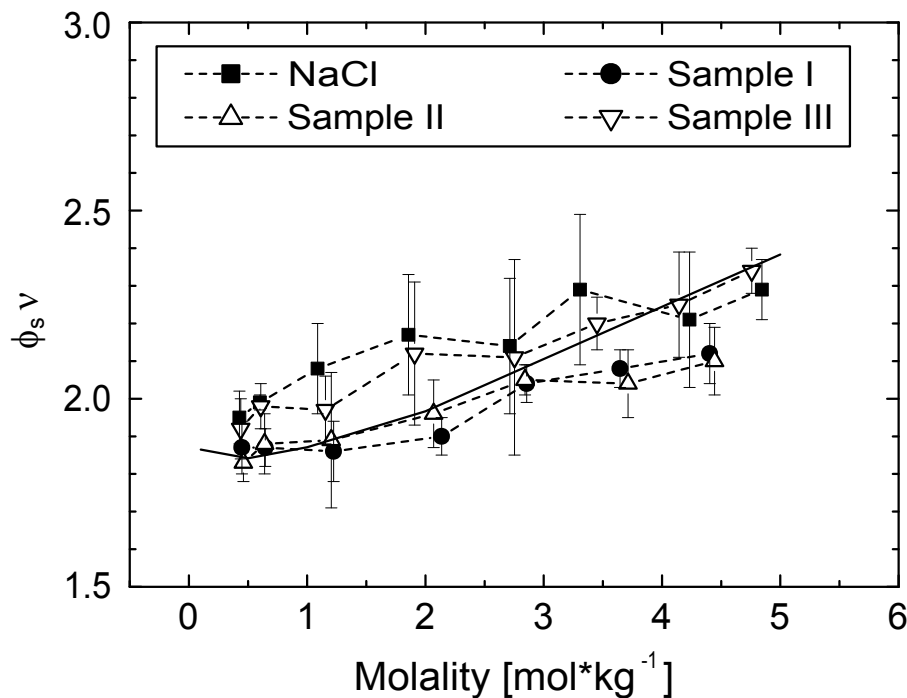
Fig. 7. $\phi_s \nu$ derived from the measured hygroscopic growth for NaCl and the three sea-salt samples in comparison to values for NaCl as given in literature (Pruppacher and Klett, 1997).
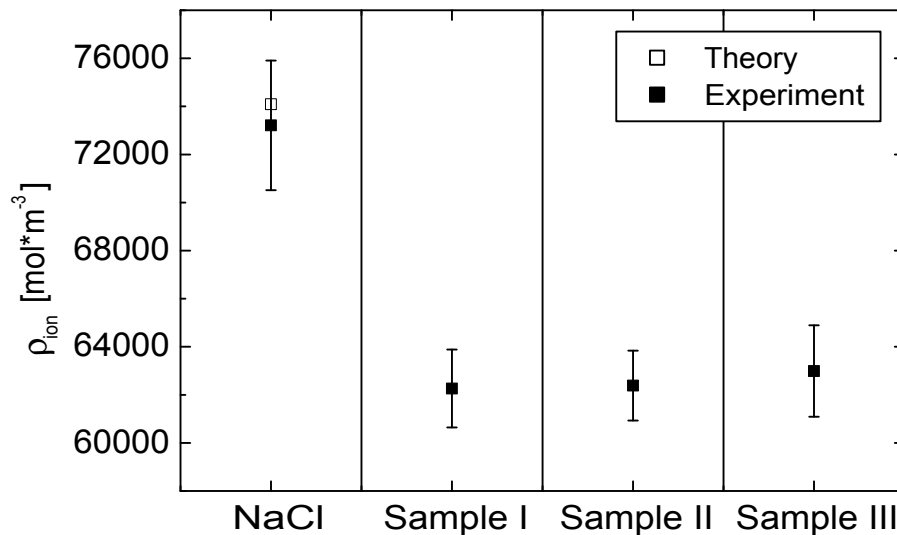
Fig. 8. The averaged values of ρ_{ion} for NaCl and the three sea-salt samples. Additionally, the theoretical value for NaCl is shown.
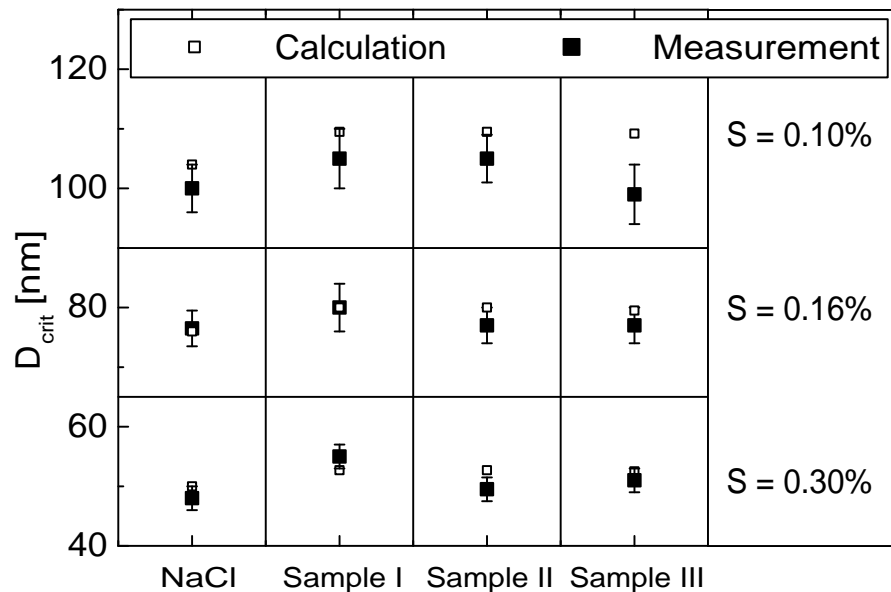
Fig. 9. Measured and calculated critical diameters for the three supersaturations.

EGU
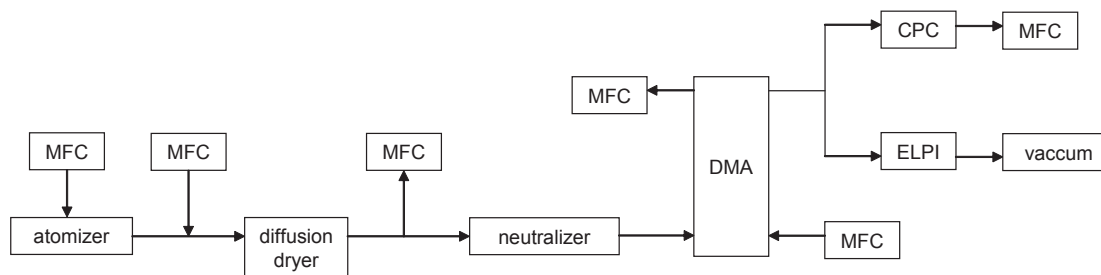
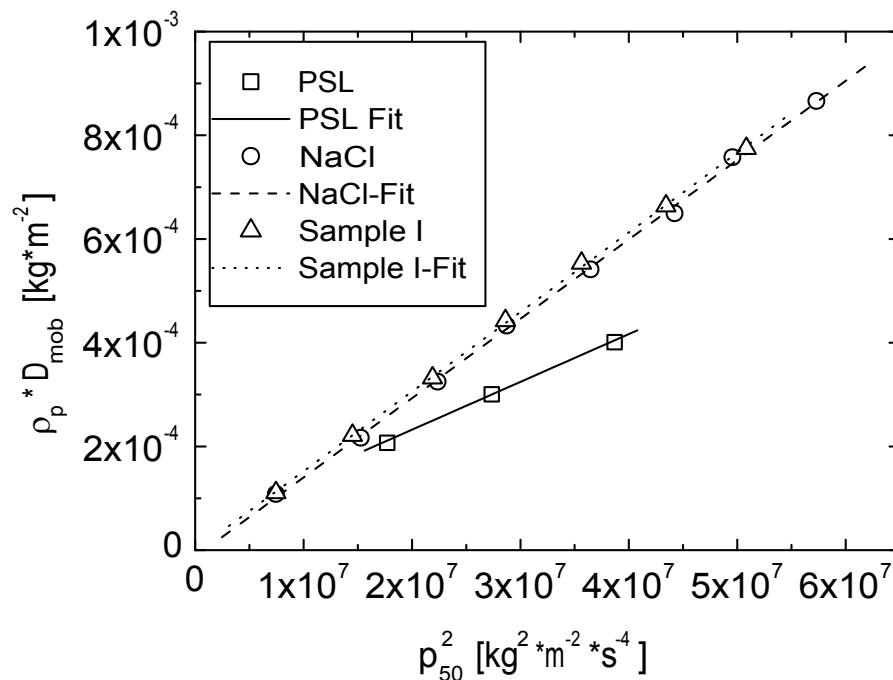**Fig. A1.** Experimental setup for the calculation of the shape factor.

Fig. A2. The product $\rho_p D_{mob}$ is plotted against p_{50}^2 for the PSL, NaCl and sea-salt (sample I) particles, to determine the shape factor of the different sea-salt particles.